Ionized Collisional Flow Model for Atmospheric RF Application

Subrata Roy[*]

Computational Plasma Dynamics Laboratory, Kettering University, Flint, MI 48504, USA

and

Datta V. Gaitonde[†]

Computational Sciences Branch, Air Force Research Laboratory, Wright Pat AFB, Ohio 45433, USA

A multi-fluid formulation is implemented to numerically model direct current (DC) and radio frequency (RF) induced plasma wall interaction. The model uses quadratic finite elements to discretize the computational space. Argon gas properties are utilized for collisionless DC glow discharge under fully ionized conditions, and the solution is compared with a theoretical model. The dielectric barrier RF discharge between two insulated electrodes uses partially ionized helium gas. The plasma, together with the charge separated sheath region, is considered collisional. The computed charge densities at the peak discharge current are compared with published numerical results. The solutions predict the ion velocity and the neutral gas density and crossflow velocity distributions. Based on the derived electric field, the transverse gas velocity solution shows the anticipated hump in the near wall profile.

Nomenclature

A	=	ionization coefficient, $cm^{-1} torr^{-1}$
B	=	ionization coefficient, $[volts/(cm\ torr)]^{0.4}$
Δ	=	increment
D_e	=	electron diffusion, cm^2/s
D_i	=	ion diffusion, cm^2/s
E	=	electric field, volts/cm
e	=	electron charge, Coulomb
f^c	=	convective flux vector
f^v	=	dissipative flux vector
i	=	iteration index
$\mathbf{M}$	=	mass matrix
M	=	ion mass
m_e	=	electron mass
m_n	=	mass of neutral gas particle
N_k	=	basis function of polynomial degree k
n_e	=	number density of electron, cm^{-3}
n_i	=	number density of ion, cm^{-3}
n_n	=	number density of neutral gas, cm^{-3}
$\hat{n}$	=	direction normal
p	=	pressure, torr
t	=	time, sec

---

[*] Associate Professor of Mechanical Engineering, 1700 West Third Avenue, and AIAA Associate Fellow.
[†] Technical Area Leader, Air Vehicles Directorate/VAAC, 2210 8th St., and AIAA Associate Fellow.

R	=	solution residual
S_e	=	assembly operator for element e
U	=	state variable
V_e	=	velocity of electron, m/s
V_i	=	velocity of ion, m/s
V_{nz}	=	axial velocity of neutral gas, m/s
$,x$	=	derivative with respect to x
z	=	ionization rate, $\sec^{-1}$
ε	=	permittivity
ϕ	=	potential, volts
κ	=	plasma resistivity
μ_e	=	mobility of electron, $cm^{2\ -1}s^{-1}$
μ_i	=	mobility of ion, $cm^2\ V^{-1}s^{-1}$
Ω	=	computational domain
Ω_e	=	computational element
ν_{en}	=	electron-neutral collision frequency
θ	=	implicitness
τ	=	phase time, sec

I.   Introduction

There is increasing interest in exploring the use of plasma actuators for active flow control in aerospace application due to several advantages. In addition to the absence of moving parts and rapid switch-on/off capabilities, electromagnetic forces have the potential to apply large forces in a relatively precise manner. Several different specific configurations have been proposed to exploit the complex interaction between the electric field and the fluid.[1-3] Recent experiments have demonstrated striking effects at both low[1,4] and high speeds.[5,6] The configurations considered include both volume and surface discharges, at pressures of atmospheric level at low speeds to O(10) torr at high-speeds. The frequency of excitation has also varied significantly, from direct current (DC) to the microwave range.   While direct current-based methods are typically employed for energy interactions with an already ionized flow, recent literature[7,8] indicates that energy budgets will depend crucially on the use of dynamic non-equilibrium ionization techniques. This follows from the fact that DC discharges operate far from the most energy efficient Stoletow point and are thus unsuitable for ionization purposes.

The focus of this effort is on methods that utilize radio frequency (RF) or low frequency methods which have seen increasing popularity in recent times. RF excitation is utilized not only as a mechanism to ionize flow volumes, but also for control itself. The experimental innovation of RF induced atmospheric uniform glow discharge (AUGD)[1,9] shows tremendous potential in the areas of electro gas dynamic flow control and energy management. In 1991, an AC voltage based method was developed[10] to produce weakly ionized plasmas which were then utilized to control flows past airfoils in low speeds (subsonic) flows.[11] Figure 1 shows schematics of RF induced atmospheric glow discharge for electrohydrodynamic (EHD) flow control. The two configurations exert paraelectric and peristaltic flow acceleration respectively at low speed with reasonable input power. According to Roth[1] the former mechanism is associated with plasma acceleration towards an increasing electric field (electrostatic body force) while the latter mechanism is predicated on traveling electrostatic wave (EHD body force) using polyphase power supply. In recent times, various configurations of dielectric barrier discharges (DBDs) have been explored[4,12-13] and significant progress has been made in describing the observed phenomena.

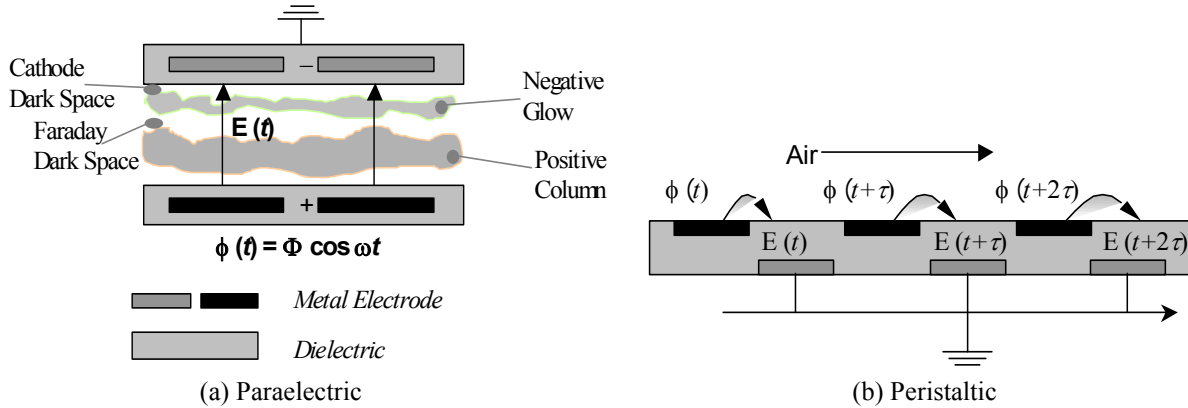American Institute of Aeronautics and Astronautics Paper No. 2004-2354

Fig. 1. RF induced atmospheric glow discharge for EHD flow control.

Low-speed flow control typically employs features of the dielectric-barrier-discharge to generate a near-surface force that can reattach separated flows.[11] One electrode is typically exposed to the flow surface, while the other is embedded in the body and displaced a short streamwise distance from it. The electric field generated by the discharge is a consequence of this geometric asymmetry as well as that associated with the vastly different mobility of the electrons and ions respectively. The net forces generated by the intermittent discharge induce ion-motion, while ion-neutral collision transfer mechanisms generate the desired surface wall-jet-like effect.

Despite increased understanding of the phenomenology, insight into the pertinent mechanisms is presently lacking. The response of the fluid to these forces requires the solution of the full equations past complex configurations under conditions where transition and turbulence are dominant. Consequently, phenomenological models have been employed for forces generated by RF discharges. For example, Shyy[12] considers a linear variation of the electric field with a constant charge density and assumptions regarding the duty cycle to obtain an expression for the force. For further progress in terms of accuracy and fidelity however, it is essential that the force model be derived from first principles through a simulation of the elementary mechanisms that yield the discharge. Such an approach can provide key information on operation; including particularly the dynamics of sheath regions where charge separation occurs, and which drive the force transfer to neutrals. With RF excitation, such regions are fundamentally different from those obtained with DC techniques, and substantially more difficult to simulate because of their unsteady nature. It is precisely the goal of this effort to set the basis for a sophisticated model, with the capability not only to reproduce the physics, but also to do so with a method that is easily extendible to complex configurations.

First-principles approaches for simulation of RF interactions with fluids remain in an early stage of development. Despite recent experimental and theoretical advances, an adequate self-consistent model describing the unsteady dynamics of critical regions of weakly ionized plasma remains a challenge. The numerical model developed in this paper includes consistent calculation of charge and neutral number densities, their momentum dynamics, electric field and potential distribution and is anchored in an efficient, robust and versatile finite-element approach. For the sake of simplicity however, we presently focus on helium, the plasma coefficients for which are relatively well known. The methodology is couched in a manner which can in principle be extended to air with the addition of new mechanisms in the source terms. The intention is to provide a tool to explore flow control concepts, develop suitable inputs for traditional fluid dynamics codes based on the Navier-Stokes equations, and to complement experimental efforts in future design and development. The powerful high-fidelity finite-element procedure was adapted from fluid dynamics to overcome the stiffness of the equations generated by multi-species charge separation phenomena. Although the primary focus is on RF discharges, several DC calculations of the traditional physical configuration of near wall electrical discharge in a practically evacuated sealed tube are also presented.

II.   Model Description

The basic theoretical details of collisional plasma-sheath with space charge effect for DC and RF power source are adopted from Ref. 14. The model is first verified for a collisionless one dimensional DC discharge problem for which the normalized equation system and its analytical solution is known.[15-16] For this case, we assume Boltzmannian distribution of electron density n_e. The ion density n_i, ion velocity V_i, magnitude of the potential ϕ and

American Institute of Aeronautics and Astronautics Paper No. 2004-2354

electric field E at steady state are predicted self-consistently from the bulk plasma to the wall using the following normalized equation set:

$$\partial_{,x}\left(n_iV_i\right) = n_e = \exp\left(-\phi\right) \tag{1a}$$

$$V_i\partial_{,x}V_i - E + V_in_e/n_i = 0 \tag{1b}$$

$$\partial_{,x}E - \kappa^2\left(n_i - n_e\right) = 0 \tag{1c}$$

$$\partial_{,x}\phi - E = 0 \tag{1d}$$

Note that the above normalized equation set assumes singly ionized plasma with ionization rate of one. For argon gas, $\kappa^{-1}=4.036\times10^{-3}$. The reported solution[15] for Eq. (1a-d) is well approximated by the plasma solution for up to $V_i < 1$.

The equations for the RF induced glow discharge through dielectric barrier do not utilize the Boltzmann equilibrium assumption for the electrons; hence the electron density is calculated. The model assumes no multiply charged ions and incorporates the following charge and neutral gas continuity equations. Poisson equation is used for calculating electric field and potential distribution.

$$\partial_{,t}n_\alpha + \partial_{,x}\left(n_\alpha V_\alpha\right) = n_e z, \quad \text{for } \alpha = e,i \quad \begin{cases} n_iV_i = n_i\mu_iE - D_i\partial_{,x}n_i \\ n_eV_e = -n_e\mu_eE - D_e\partial_{,x}n_e \end{cases} \tag{2a}$$

$$\partial_{,t}n_n + \partial_{,x}\left(n_nV_{nz}\right) = -n_e z \tag{2b}$$

$$\varepsilon\partial_{,x}E - e\left(n_i - n_e\right) = 0 \tag{2c}$$

$$\partial_{,x}\phi + E = 0 \tag{2d}$$

The electron diffusion is obtained from Einstein relation, $D_e=(T_e/e)\mu_e$, where T_e is the energy in electron volts, e is the elementary charge and $\mu_e=e/(m_e\nu_{eh})$ is mobility of an electron, where $\nu_{en}\approx10^{12}$/s is the electron-neutral collision frequency.[17] The ion diffusion $D_i=500$ cm^2/s at 300K, and the ion mobility μ_i is given as:[18]

$$p\mu_i = 8\times10^3\left(1-8\times10^{-3}E/p\right) \text{ cm}^2\text{V}^{-1}\text{s}^{-1}\text{torr, for } E/p \le 25 \text{ V cm}^{-1}\text{torr}^{-1}$$

$$p\mu_i = \frac{4.1\times10^4}{\sqrt{E/p}}\left(1-\frac{27.44}{\left(E/p\right)^{3/2}}\right) \text{ cm}^2\text{V}^{-1}\text{s}^{-1}\text{torr, for } E/p > 25 \text{ V cm}^{-1}\text{torr}^{-1} \tag{3}$$

In (3), E is the electric field magnitude and p is the pressure. The ionization rate z for helium gas used here is:[14]

$$z = \text{A}\exp\left(\frac{-\text{B}}{\left(E/p\right)^{0.4}}\right)p\mu_eE \text{ s}^{-1}; \quad \text{A} = 4.4 \text{ cm}^{-1}\text{torr}^{-1} \text{ and B} = 14 \text{ [V/(cm torr)]}^{0.4} \tag{4}$$

where, n_e is the electron number density.

The effect of the excitation on the neutrals is simulated by considering a separate momentum equation for the crosswise neutral gas velocity, V_{nz}, for this species.

$$\left(\partial_{,t} + \partial_{,x}V_{nz}\right)V_{nz} = -\left(1/2m_nn_n\right)\partial_{,x}\left(\varepsilon E^2\right) + \left(m_e/m_n\right)\nu_{en}\left(V_e - V_{nz}\right)$$
$$+ \left(M/m_n\right)\nu_{in}\left(V_i - V_{nz}\right) + n_ezV_i/n_n. \tag{5}$$

Here, m_e, M and m_n are mass of electron, ion and neutral respectively, ε is the permittivity, V_i and V_e are ion and electron velocities, while ν_{en} and ν_{in} are the electron-neutral and ion-neutral collision frequencies, respectively. The model assumes that $\partial_x \gg \partial_z$ and terms involving the effect of electrons and neutrals are modeled in the standard manner. In the absence of other external forces, as a first approximation, it is assumed that the hydrodynamic and electrostatic pressure gradients are in approximate equilibrium.[1] This assumption, although not appropriate at collision rates representative of low pressures, is reasonable at the present study, which considers atmospheric conditions.

III. Numerical Method

The Finite element (FE) techniques are well known for their adaptability to arbitrary multidimensional geometries and boundary conditions. Here, a 1D finite element formulation is employed to solve Eqs. (1a-d), (2a-d),

and (5) which may be expressed as $L(\mathbf{U})=0$, where $\mathbf{U}$ contains all state variables, *e.g.*, ion density, ion velocity and potential, and L is a differential operator. The weak statement associated with a variational integral underlines the development of this numerical algorithm. The physical domain is spatially semi-discretized (^{h} approximated) using generic computational domain, *i.e.*, the finite element. The state variables are interpolated inside the element, via the trial space FE basis set $N_k(x_j)$ that typically contains Chebyshev, Lagrange or Hermite interpolation polynomials complete to degree k. The spatially semi-discrete FE implementation of the *weak statement* WS^h for $L(\mathbf{U})=0$ leads to

$$\mathrm{WS}^h = S_e \left(\int_{\Omega_e} N_k L_e(\mathbf{U}) d\tau \right) \equiv 0$$

$$= S_e \left(\int_{\Omega_e} N_k \frac{d\mathbf{U}}{dt} + \int_{\Omega_e} N_k (s) d\tau + \int_{\Omega_e} \frac{\partial N_k}{\partial x_j} \left(\mathrm{f}_j - \mathrm{f}_j^v \right)_e d\tau - \int_{\partial \Omega_e \cap \partial \Omega^h} N_k \left(\mathrm{f}_j - \mathrm{f}_j^v \right)_e \hat{n}_j d\sigma \right) \quad (6)$$

S_e symbolizes the "assembly operator" carrying local (element e) matrix coefficients into the global arrays, s is a source term (e.g. zn_e in Eq. (1)) and f^c and f^v are convective and disspative flux vectors, respectively, and $\hat{n}$ is the direction normal. Application of Green-Gauss divergence theorem in (6) yields natural homogenous Neumann boundary conditions. The surface integral in the second line of (6) contains the (un)known boundary fluxes wherever fixed or flux boundary conditions are enforced.

Independent of the physical dimension of Ω, and for general forms of the flux vectors, the semi-discretized weak statement always yields an ordinary differential equation (ODE) system that is fully discretised using a θ–implicit or τ-step Runge-Kutta type time integration procedure. The terminal ODE is usually solved using a Newton-Raphson scheme for $\mathbf{U}(t)$:

$$\mathbf{U}_{\tau+1}^{i+1} = \mathbf{U}_{\tau+1}^{i} + \Delta \mathbf{U}^i = \mathbf{U}_\tau + \sum_{p=0}^{i} \mathbf{U}^{p+1}, \text{ where}$$

$$\Delta \mathbf{U}^i = -\left[\mathbf{M} + \theta \Delta t (\partial \mathbf{R} / \partial \mathbf{U}) \right]^{-1} \mathbf{R}(\mathbf{U}) \quad (7)$$

Here, a $\tilde{\ }$ implicit time marching procedure is employed. In (7), $\mathbf{M} = S_e(\mathbf{M}_e)$ is the "mass" matrix associated with element level interpolation, $\mathbf{R}$ carries the element convection, diffusion and source information. The calculation of the "Jacobian" $\partial \mathbf{R}/\partial \mathbf{U}$ and inversion of the $\mathbf{M}+\theta\Delta t(\partial \mathbf{R}/\partial \mathbf{U})$ matrix with sufficient accuracy is obviously a numerical challenge. However, unlike the traditional finite difference/volume methods, the present FE algorithm allows one to simulate the system simultaneously without requiring any sub-iteration for the Poisson solver.

Further details of the code are described in Refs. 19-20. The solution is convergent at any given timestep when the maximum value of the residual relative norm for each of the state variable becomes smaller than a chosen convergence criterion of 10^{-4}. It is declared steady state as the transient features die down and the solution any timestep converges to the 10^{-5} within the first iteration.

IV.   Results and Discussion

The combined plasma-sheath dynamics is modeled on a one-dimensional geometry. Equation sets (1a-d), (2a-d) and (5) are solved using second order time accurate implicit ($\theta = 1$) finite element method over a computational domain (x:0, x_w). Two cases are simulated for verification and benchmarking of the algorithm with available results. The first considers the DC-discharge, for which the Sternberg solution[15] is employed in the collisionless assumption. The ion density and velocity at the center of the plasma ($x=0$) were set to be 1 and 0, respectively, while the electric field and potential of the bulk were both set to be zero. The configuration for RF discharge through the dielectric barrier (DB) is similar to the paraelectric case in Fig. 1a. The left electrode is grounded while a RF alternating frequency of 50 kHz with rms potential of 1.2 kV is imposed at the right electrode. The electrodes are coated with 0.6mm alumina and are kept at a 5mm gap distance from each other. Electrons are assumed to be isothermal at the boundary and maintained at 1eV (~11,600K) while the ions are cold (300K) at 300 torr. All other boundary conditions are maintained at zero flux, i.e., homogeneous Neumann boundary conditions are applied. The solutions are verified by comparison with the reported results of Massines et al.[13] The results are then employed to explore the enhancement of near wall neutral velocity. This model presently does not include secondary emission.

A. DC Discharge Simulations

We first solved the DC plasma-wall equation on 100 uniform quadratic elements (201 equidistant points). Sternberg and Godyak[15] derived the analytical solutions for this problem from the center of plasma till the region

where ion Bohm velocity is reached. Figure 2a-d shows excellent comparison of the simulation prediction for ion number density, velocity, electric field and potential distributions for $\kappa^2 = 61390$ with the published results[16] for a normalized wall potential of 50. The wall is located at a normalized $x_w = 0.71147$. The solution from Ref. 16 is plotted on every 3% distance of the domain for visual clarity. Figure 2 also shows the effect of nondimensional permittivity κ^{-1} on the state variables. As κ^2 increases from 6139 to 61390, the ion density decreases from 0.2 to 0.05 in Figure 2a and the ion velocity increases from 3 to 10 in Figure 2b. The effect is evident in Figures 2c and 2d showing nearly tenfold increase in the magnitude of the wall potential and electric field, respectively. Figure 3a also plots the growth of the sheath as the Boltzmannian electron number density bifurcates near $(\pi/2 - 1)$ from the ion number density solution for $\kappa^2 = 61390$. The location of this sheath edge is also noticeable for ion velocity, potential and electric field distribution in Figures 2b-d.
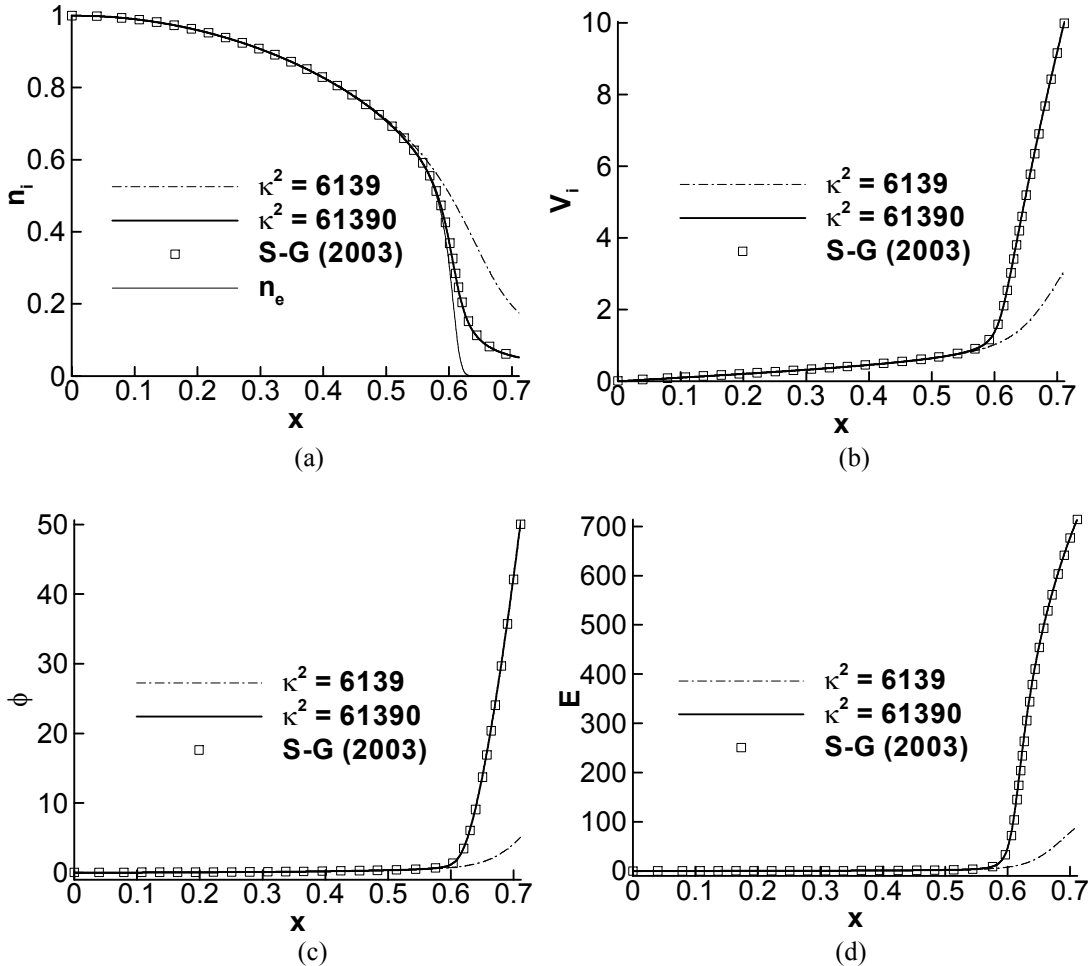

(a)

(b)

(c)

(d)

Figure 2. DC sheath solution compared with Ref. 15. (a) Ion number density, (b) ion velocity, (c) magnitude of the potential and (d) electric field distribution.

B. RF Dielectric Barrier Discharge

For benchmarking with the solution reported by Massines et al.[13], all numerical results presented here are at 9.3 μs where the discharge current is the maximum. The mesh consists of 200 equal length 1D quadratic finite elements (i.e., 401 nodes). The algorithm is spatially third order accurate. The applied rms voltage and forcing frequency are 1.2 kV and 50 kHz, respectively.

Numerical prediction for the ion number density distribution plotted in Fig. 3a using the finite element procedure demonstrates noticeable similarity with previously reported results.[13] The peak of ion number density near the instantaneous cathode is 6×10^{17} m^{-3} which is 16% higher than that previously reported. Corresponding electron number density shown in Fig. 3b also compares within +18% disparity with published results[13] in charge prediction. Evidently, electron number density starts to decrease rapidly near the plasma-sheath boundary and becomes almost zero at the instantaneous cathode. This is expected due to the build up of a strong negative potential at the wall,

American Institute of Aeronautics and Astronautics Paper No. 2004-2354

causing electrons to be expelled from the presheath-sheath region and only supra-thermal electrons to be able to overcome the potential barrier and cross over to the wall. The number of supra-thermal electron is always small in any given plasma. The neutral number density decays due to the ionization process in RF glow discharge. Noticeably the neutral density (not shown) reduces from 2×10^{19} m^{-3} by an order of magnitude in the region where maximum charge is produced. However, the gas density does not increase as the charge density decreases primarily due to the absence of recombination in the present model (see Eq. 2b). The dielectric does not allow charges to move along it, so recombination may be delayed.

The computed electric field $E = -\partial_{,x}\varphi$ is plotted in Fig. 4 and shows high positive gradients near both electrodes. Interestingly the field becomes negative predicting a sharp drop of potential near the anode (fall) and the same effect will be expected near the cathode. This phenomenon is due to electron waves and is well explained by Raizer et al..[21] An electrical double layer is also noticeable near the grounded electrode. For exploratory purposes, the neutral gas flow in the crosswise direction is also predicted using the assumptions noted earlier. Although this assumption is based on relatively simplistic reasoning and apparently valid, only for 1-D situations[4] it implicitly factors the charge distribution through the electric field gradient and serves as a simple method of extracting a body force from the computed electric field. Within these limitations, the crossflow gas velocity calculated using Eq. 5 is plotted in Fig. 6a shows reasonable trend in comparison to the test data in Fig. 5b reported by Roth.[1] The purpose of the figure is to show the similarity of computed and experimental profiles demonstrating the augmentation of near-wall momentum to yield a wall-jet-like structure through a first principles approach. The similar quantitative values of the maxima are likely fortuitous, since they consider different fluids under different physical setups. The large electric field gradients near each electrode are associated with charge separation consistent with the different local ion and electron densities. The net force, related to the product of this charge and the electric field, peaks near each electrode. The computed crosswind thus shows two peaks, one near each electrode. However, due to higher electric field the velocity near the instantaneous anode is 1/5th of that near the cathode, Fig. 5a. The parameters chosen for the simulation yield relatively low induced velocities. Experimental evidence[4,22] suggests that proper placement of such control devices in critical fluid dynamic regions can further leverage the EHD effect by influencing the bifurcation, for example, through suppression of separation, and a fundamental change in the topology. Nonetheless, methods of increasing the induced velocity must be explored in the context of scalability issues, which remain to be resolved.
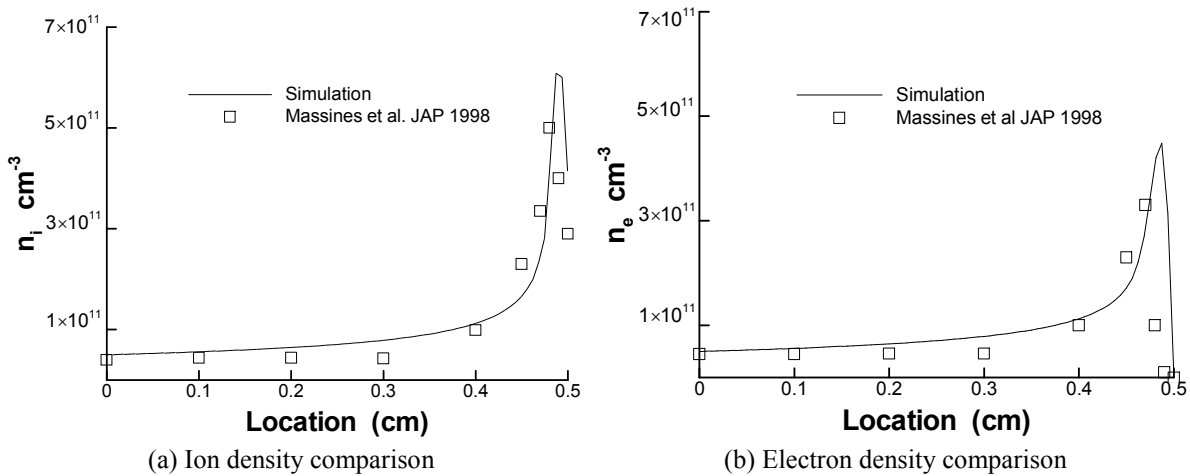

(a) Ion density comparison   (b) Electron density comparison

Figure 3. RF glow discharge solution at maximum discharge current.
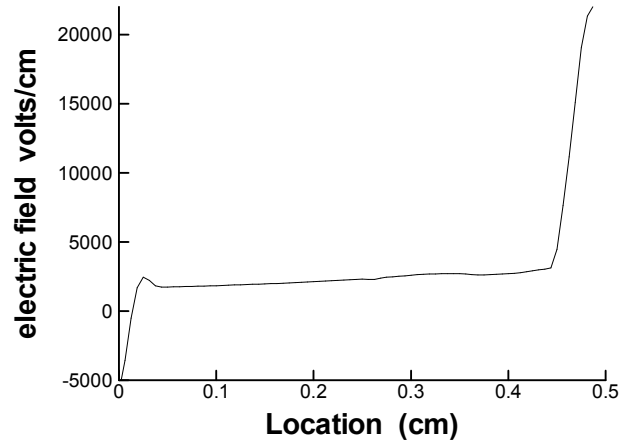
Figure 4. Electric field distribution between the electrodes at the peak discharge current.

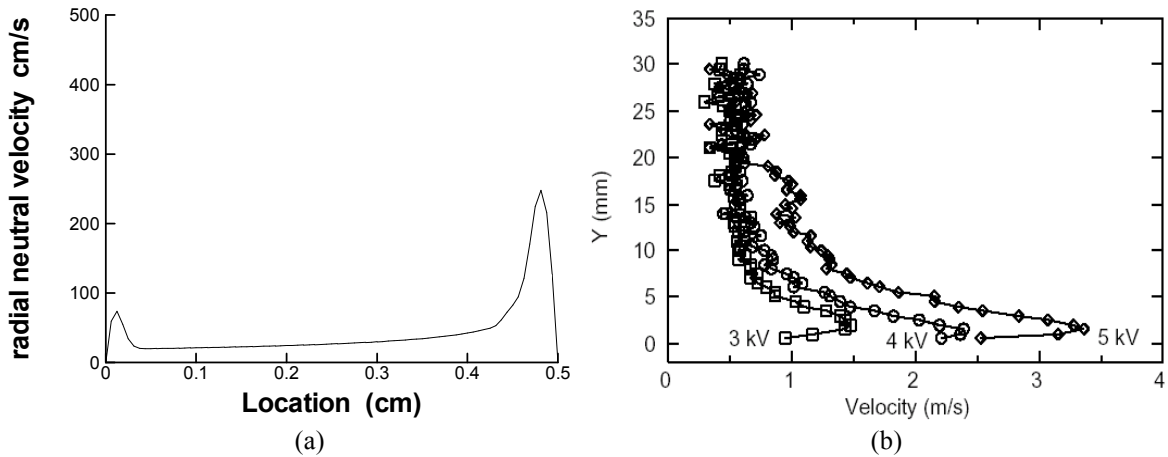(a)   (b)

Figure 5. Neutral gas velocity distribution. (a) Calculated magnitude of crosswise component of the gas velocity distribution, (b) Experimental velocity distribution normal to the surface (Roth[1]).

V.   Conclusion

A finite element based formulation of plasma–fluid interactions is given for a partially ionized plasma using the multi-component fluid equation. The model is applied for simulating atmospheric RF glow discharge for partially ionized helium gas between two electrodes. The computed solutions for charge densities, the ion velocity and the neutral gas density and crossflow distributions show anticipated trends. Specifically, ion and electron number densities at the peak discharge current are compared with published numerical results. The electric field driven radial neutral gas velocity compares well with available experimental data. Future research goals include extension to multi-dimensional configurations, with emphasis on simulation of surface RF discharges, identification of critical physical processes in RF-based EHD, development of a theoretical model for air of suitable complexity and finally implementation into a powerful, robust and efficient numerical tool. The application of the methodology in understanding the relative importance of Lorentzian momentum transfer versus Joule heating will be particularly useful in determining the effectiveness of RF-based plasma flow control at higher speeds, where compressibility is important. The present effort also sets the stage for exploration in the higher-frequency range encompassing the microwave regime, where substantially higher power levels may be brought to bear.

References

[1] J.R. Roth, Phys. Plasmas, **10**, 2117 (2003).

[2] E.P. Gurijanov and P.T. Harsha, AIAA Paper no. 96-4609 (1996).

[3] Y.C. Ganiev, V.P. Gordeev, A.V. Krasilnikov, V.I. Lagutin, V.N. Otmennikov and A.V. Panasenko, J. Thermophysics and Heat Transfer, **14**, 10 (2000).

[4] C.L. Enloe, T.E. McLaughlin, R.D. VanDyken, K.D. Kachner, E.J. Jumper and T.C. Corke, *41st AIAA Aerospace Sciences Meeting*, Paper No. 2003-1021 (2003).

[5] R.B. Miles, AIAA Paper No. 2000-2324 (2000).

[6] S.B. Leonov and V.A. Bityurin, AIAA-2002-5209 (2002).

[7] Adamovich, I.V., Subramaniam, V.V., Rich, J.W. and Macheret, S.O., AIAA Journal, **36**, 816 (1998).

[8] Macheret, S. O., Shneider, M. N., and Miles, R. B., Journal of Propulsion and Power, **18**, 424 (2002).

[9] G.A. Hebner, J.T. Verdeyen and M.J. Kushner, J. Appl. Phys., **63**, 2226 (1988).

[10] N. Kanda, M. Kogoma, H. Jinno, H. Uchiyama and S. Okazaki, Proc. 10th Symp. on Plasma Chem., Vol. 3, Paper no. 3.2-20 (1991).

[11] T.C. Corke, E.J. Jumper, M.L. Post, D. Orlov and T.E. McLaughlin, *40th AIAA Aerospace Sciences Meeting*, Paper No. 2002-0350 (2002).

[12] W. Shyy, B. Jayaraman and A. Andersson, J. Appl. Phys., **92**, 6434 (2002).

[13] F. Massines, A. Rabehi, P. Decomps, R.B. Gadri, P. Ségur and C. Mayoux, J. Appl. Phys., **83**, 2950 (1998).

[14] S. Roy, B.P. Pandey, J. Poggie and D. Gaitonde, Physics of Plasmas, **10**, 2578 (2003).

[15] Sternberg, N. and Godyak, V. A., IEEE Trans. On Plasma Sci., **31**, 665 (2003).

[16] J. Poggie and N. Sternberg, AIAA-2004-0177 (2004).

[17] K. Akhtar, J.E. Scharer, S.M. Tysk and E. Kho, Review of Scientific Instruments, **74**, 996 (2003).

[18] L. Ward, J. Appl. Phys. **33**, 2789 (1962).

[19] S. Roy and B.P. Pandey, Journal of Propulsion and Power, **19**, 964 (2003).

[20] D. Balagangadhar and S. Roy, Computer Methods in Applied Mechanics and Engineering, **190**, 5465 (2001).

[21] Raizer, Y.P., Shneider, M.N. and Yatsenko, N.A., Radio-Frequency Capacitive Discharges, CRC Press, London, p. 292, 1995.

[22] L.S. Hultgren and D.E. Ashpis, AIAA-2003-1025 (2003).